

LEVEL SET BASED RECONSTRUCTION ALGORITHM FOR EIT LUNG IMAGES

Peyman Rahmati¹, Manuchehr Soleimani², and Andy Adler¹

¹Carleton University, Ottawa, Canada. {prahmati,adler}@sce.carleton.ca

²Bath University, UK. {m.soleimani}@bath.ac.uk

ABSTRACT

We show that electrical impedance tomography (EIT) image reconstruction algorithms based on the Level Set (LS) method are suitable for real data, which is breathing data in our application. The LS based reconstruction method (LSRM) helps track fast topologically changing interfaces, which are typically smoothed by traditional voxel based reconstruction method (VBRM), during the monitoring process. We represent lung images by applying the LSRM using difference solver and then compare the results with the VBRM. According to our results, LSRM outperforms its voxel based counterparts in producing high quality, high contrast images of lung.

Index Terms— Inverse Problem, Electrical Impedance Tomography, Image Reconstruction Algorithm

1. INTRODUCTION

Tomographic imaging systems seek to see the inside objects, by introducing energy and measuring its interaction with the medium. Electrical Impedance Tomography (EIT) measures the internal impedance distribution using surface measurements. Electrical current is applied to the medium and the voltage at the surface is measured using electrodes. The impedance distribution is then estimated based on the measured voltages and medium geometry. Some of typical applications of these techniques are for geophysical imaging [1, 2, 3], process monitoring [4, 5], and functional imaging of the body [6, 7].

In this paper, we focus on image reconstruction in EIT using the level set approach. The level set approach has become popular because of its ability to track propagating interfaces [8, 9], and more recently it has been applied in variety of applications in inverse problems and in image processing [10, 11, 12, 13]. Level set based reconstruction method (LSRM) is a nonlinear inversion scheme using an optimization approach to iteratively reduce a given cost functional, which is the norm of the difference between the simulated and measured data. In comparison to the voxel based reconstruction method (VBRM) (e.g. [14]), the LSRM has the advantage of introducing the conductivity of background and that of inclusions as known priori information into the reconstruction algorithm, enabling it to reconstruct sharp contrasts [4]. The unknown parameters to be recovered from the data are the size, number, shapes of the inclusions. These unknown parameters are given as the zero level set of a higher dimensional function, called level set function. In every iteration, the level set function (LSF) is modified according to an update formula to modify the shape of the inclusion at its zero level set (see fig. 1).

The level set method for shape based reconstruction is well studied in electrical and electromagnetic imaging for sim-

ulated data [10, 11, 12, 15, 16, 17, 18, 19]; however, it has been seldom shown to be used for human data. This study is the first implementation of LSRM for EIT breathing real data demonstrating the results of applying a difference solver.

The remainder of the paper is organized as follows: in the next section, we formulate level set approach using difference solver for EIT; in section 3, we introduce into the level set technique employed for solving the inverse problem of EIT lung images; the experimental data is represented in section 4; in section 5, we evaluate the performance of LSRM for lung monitoring data and compare LSRM to VBRM; and finally section 6 presents discussions and conclusions.

2. DIFFERENCE AND ABSOLUTE RECONSTRUCTION METHODS

There are two primary reconstruction types in EIT: "absolute (static) imaging" which attempts to recover an estimate of the absolute conductivity of the medium from the achieved data frame, and "difference imaging" which attempts to recover an estimate of the change in conductivity between two times based on the change between two data frames, v_2 and v_1 . Difference EIT can compensate for measurement errors which do not change between data frames. Difference EIT is based on a difference data vector, $[y]_i = [v_2]_i - [v_1]_i$ or, in order to decrease measurement noise, the normalized difference data $[y]_i = [v_2]_i - [v_1]_i / [v_1]_i$. Using a finite element model (FEM), the medium is discretized into N elements with conductivity σ . The conductivity change vector $x = \sigma_2 - \sigma_1$ is the change between the present conductivity distribution, σ_2 , and that at the reference measurement, σ_1 . The linearized difference forward solution for small changes in conductivities over time is given by [20]:

$$y = J\hat{x} + n, \quad (1)$$

where J is Jacobian or sensitivity matrix around the reference conductivity distribution, defined by $\frac{\partial y}{\partial x}|_{\sigma_1}$ and n is the measurement noise, typically assumed to be an uncorrelated white Gaussian noise. In an EIT application where the conductivity of the medium (\hat{x}) is unknown, we need to solve an inverse problem to find an estimate of the conductivity, referred to as \hat{x} . The most common approach to find \hat{x} is the use of the Gauss-Newton (GN) algorithm for EIT reconstruction [21, 22]. The GN method solves the EIT inverse problem by minimizing the following quadratic residue [20]:

$$\|y - J\hat{x}\|_{\Sigma_n}^2 + \|\hat{x} - x_0\|_{\Sigma_x}^2, \quad (2)$$

where Σ_n^{-1} and Σ_x^{-1} are the covariance matrix of measurement noise and that of conductivity vector (\hat{x}), respectively; and x_0 represent the expected value of element conductivity changes. By solving (2) for \hat{x} , the linearized EIT inverse solution is obtained as [20]:

$$\hat{x} = (J^T J + \lambda^2 R)^{-1} J^T y, \quad (3)$$

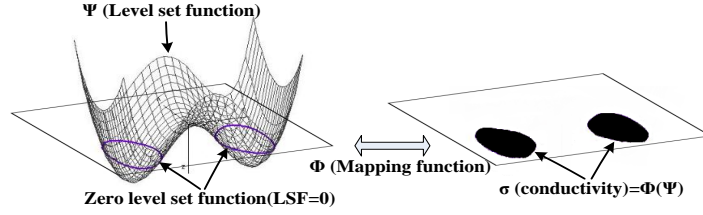


Fig. 1: LSF mapping to a 2D plane. From left to right columns, The 3D representation of an arbitrary LSF and its zero level set function crossing zero level set surface, and 2D mapping of the LSF on the zero level set surface.

where R is the regularization matrix and λ is the regularization hyperparameter to which can control the trade off between resolution and noise attenuation in the reconstructed image. In the remainder of this paper, the GN approach is considered the reference technique. GN image reconstruction is understood to result in smoothed images, since the regularization matrix is typically based on a penalty filter for non-smooth images.

3. LEVEL SET METHOD

One effective method to allow the reconstruction of sharp images is the Level Set method [12]. The classic formulation of this method assumes that the reconstructed image can take only two conductivity values: one for background with value σ_b and another one for inclusions with value σ_i . The regions which form the background and the inclusions are defined by a LSF, Ψ : a signed distance function to identify the unknown interface between the two conductivities. The value of the LSF is zero on the interface, negative inside the interface, and positive outside.

Compared to the more typical VBRMs, the LSRMs are more accurate reconstruction of objects with high step change of conductivity at the interface (high contrast objects). This is because most regularization schemes for the traditional methods, which are necessary for stabilizing the inversion, have the side-effect of artificially smoothing the reconstructed images. Therefore, these schemes are not well-suited for reconstructing high contrast objects with sharp boundaries.

In order to arrive at a robust and efficient shape-based inversion method, a powerful technique needs to be incorporated for computationally modelling the moving shapes. Level set technique [8, 9] is capable of easily modeling the topological changes of the boundaries. The LSRM has been shown the capability of being suitable for reconstructing object with fast changes at its interface over time, applicable to EIT in brain for cryosurgery monitoring [4]. Fig. 1 shows a two phases image reconstructed using the LSRM. The LSF Ψ has separated the zero level set surface into two regions: foreground (inclusions) and background. The mapping function Φ projects the LSF to a 2D mesh to be applied for inverse solution calculation using FEM. Fig. 1, right panel, shows the conductivity of the inclusions in black where the LSF is negative and that of background in white where the LSF is positive. To begin with, we need to define an initial LSF, which may be a circle on level zero; and then deform this initial LSF using a predefined energy functional iteratively. Fig. 2 represents the steps as k represents the iteration number. After

defining the initial LSF, the mapping function Φ projects the LSF to a 2D mesh to be fed to difference solver block to calculate the system sensitivity matrix, Jacobian (J_k), as well as element differential potential vectors, Δd_i . The next step is to update the energy functional which is Gauss-Newton formula, ΔLSF_k . The initial LSF is then deformed by ΔLSF_k generating a new LSF. This new LSF is fed again to difference solver block for another iteration if the current iteration number (k) is not bigger than a maximum iteration number (K). In the following, we discuss about the mathematical presentation of the LSRM.

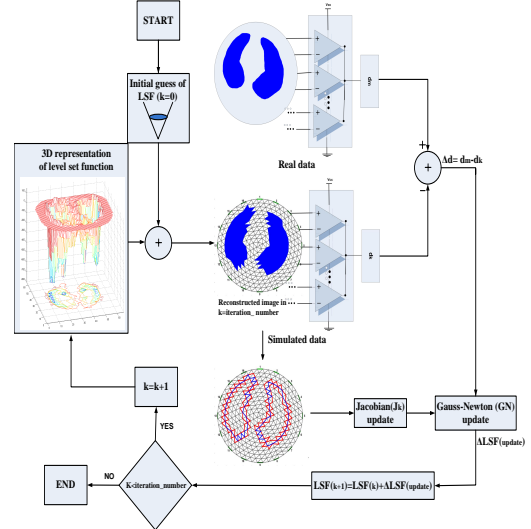


Fig. 2: The level set based reconstruction algorithm using difference solver. Steps from top to down: LSF initial guess, inverse difference solver, Gauss-Newton update, LSF displacement by the given update, and iteration number increment.

In this technique, the shapes which define the boundaries, are represented by the zero level set of a LSF Ψ . If D is the inclusion with conductivity σ_i embedded in a background with conductivity σ_b , the boundary of the inclusion, which is also an interface between two materials, is given by the zero level set [17]:

$$\partial D := \{r : \Psi(r) = 0\}, \quad (4)$$

where the image parameter at each point r is [17]

$$\sigma(r) = \begin{cases} \sigma_i & \text{for } \{r : \Psi(r) < 0\}, \\ \sigma_b & \text{for } \{r : \Psi(r) > 0\} \end{cases} \quad (5)$$

If we change this LSF for example by adding an update, we move the shapes accordingly. This update to a given LSF causes the shapes being deformed in a way which reduces an error residue (cost functional).

The LSRM combines the general idea of GN optimization approach with a developed shape-based inversion approach. In order to mathematically derive the LSRM, we define the mapping (Φ) which assigns a given LSF Ψ_D to the corresponding parameter distribution by $\sigma = \Phi(\Psi_D)$. The parameter distribution σ has the same meaning as in the traditional GN inversion scheme. The only difference is that in the shape-based situation it is considered as having only two values, namely an "inside" value and an "outside" value. In shape-based reconstruction approach, We are looking for the LSF Ψ_D which have finally divided the image into two separate areas as foreground (inclusion) and background.

Having defined this mapping Φ , we can now replace the iterated parameter σ_n by $\sigma_n = \Phi(\Psi_D) = \Phi(\Psi_n)$. Instead of the forward mapping $F(\sigma)$, we need to consider now in the new GN type approach the combined mapping [17]:

$$d(\Psi) = G(\Phi(\Psi)), \quad (6)$$

where d is data point, G is system matrix, and $\Phi(\Psi)$ stands for conductivity, see fig. 1.

According to the chain rule, the level set (LS) sensitivity matrix can be written as below:

$$\begin{aligned} \text{Sensitivity} = J_{LS} &= \frac{\partial d}{\partial \Psi} = \left(\frac{\partial G}{\partial \Phi(\Psi)} \right) \left(\frac{\partial \Phi(\Psi)}{\partial \Psi} \right) \\ &= (J_{GN})(M), \end{aligned} \quad (7)$$

where $\frac{\partial G}{\partial \Phi(\Psi)}$ stands for the traditional GN sensitivity matrix (J_{GN}), and $\frac{\partial \Phi(\Psi)}{\partial \Psi} = M$ is the matrix representing the mapping function ($\Phi(\Psi)$). Then, the new GN update is [17]:

$$\begin{aligned} \Psi_{k+1} &= \Psi_k + \dots \\ \lambda \left[(J_{(LS,k)}^T J_{(LS,k)} + \alpha^2 L^T L)^{-1} (J_{(LS,k)}^T (d_{real} - d(\Psi_k))) \right] \dots \\ &- [\alpha^2 L^T L (\Psi_k - \Psi_{int})] = \Psi_k + GN_{update} \\ &= LSF(k) + \Delta LSF, \end{aligned} \quad (8)$$

where Ψ_{int} in the update term corresponds to the initial estimate of the LSF. There are two parameters λ and α to be tuned in this level set formulation.

Fig. 2 illustrates the algorithm to calculate the above update formula. The optimal choice of the two parameters, λ and α , depends on the mesh density, the conductivity contrast and the initial guess [4]. The length parameter λ determines the magnitude of the LSF displacement, changing the shape of inclusion, in a given update. The higher the λ , the higher the LSF displacement will be. The effect of the regularization parameter α depends on the choice of the regularization operator L . An identity matrix for L increases the stability of the inversion due to not smoothing out the LSF. However, a first order difference operator for L will smooth the LSF [4]. As α increases, the smoother the final LSF tends to be. A large value for α disturbs the reconstruction algorithm to separate close objects to each other properly (low distinguishability). To have a better distinguishability, in our experiments shown in the following section, we will choose L to be the identity operator. This allows us to better separate different objects

from each other. In our results, we have put a value of zero for our initial guess of Ψ_{int} in the above shape-reconstruction form.

4. EXPERIMENTAL DATA AND RESULTS

Human breathing data were acquired from a healthy young male subject during normal breathing while seated. Electrodes were placed around the chest at the 6th intercostal space. EIT surface potential data corresponds to end-expiratory, and end-inspiratory cycles. Images were reconstructed on a mesh roughly conforming to the anatomy of the subject.

We tested the suitability of the LSRM for lung data using the breathing data. Fig. 3 shows the reconstructed images for one stage of breathing cycle using either the VBRM or the LSRM. The reconstructed image by the LSRM represents the air distribution inside the lungs after 10 iterations (fig. 3(c)). As inspired air increases, the resistivity of the lungs increases which has been shown as blue regions in the reconstructed images in fig. 3. The reconstructed images show the superiority of the LSRM with respect to the VBRM in terms of creating sharper reconstructions with larger contrasts at the interface between the inclusion and the background, presenting step change of conductivity.

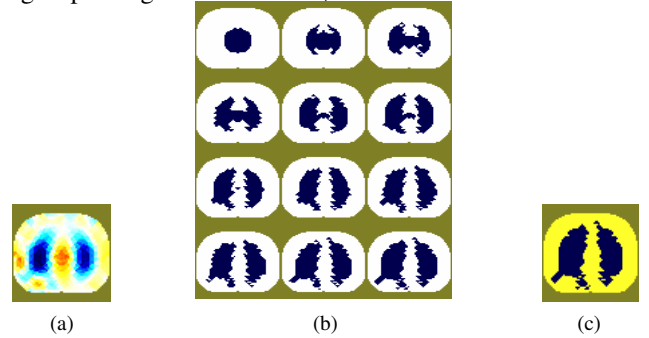


Fig. 3: level set based reconstruction algorithm using a difference solver for breathing data (scale=1). (a) The lung reconstructed image using GN approach. (b) The iterations of the LSRM for the same lung image in (a). (c) The final lung reconstructed image using the LSRM.

5. CONCLUSION AND DISCUSSION

We proposed the LSRM in difference mode for real data of breathing, which have not already been investigated for EIT. The inverse solution of Gauss-Newton formula updates the sensitivity matrix and consequently the LSF with every iteration, dividing the medium into two maximally homogeneous areas; the foreground and the background. The LSRM depicts the capability of finding the big conductivity changes at the interface between lung and the background (fig. 3). Due to the update sensitivity matrix has been calculated on a narrow band region, involving the elements sharing an edge with the interface between foreground and background (see fig. 2), the LSRM is faster and less computationally expensive comparing with the VBRM.

There are many cases of inverse problems where more than two phases need to be reconstructed from given data.

For these applications, novel level set descriptions have to be developed to model these multi-phase situations in an efficient way, such as the Color level set technique [23]. In the original color level set technique, n LSFs are used in order to describe the evolution of up to $m = 2n$ different phases. This approach has also been investigated more theoretically in [24]. Irishina et al. in [25] described four different breast tissue types (skin, fatty tissue, fibroglandular tissue and a possible hidden tumor) by three different LSFs in a modified color level set representation for the application of early breast cancer detection. In this work, the theoretically possible $2^3 = 8$ different characteristic tissue values are enforced to fall into 4 different groups of characteristic tissue values.

Our results represents that the LSRM is suitable to be applied for EIT real data of breathing (fig. 3); Comparing with the VBRM, the LSRM shows high quality and high contrast lung images.

6. REFERENCES

- [1] Loke M H, and Barker R D 1996a *Rapid least-squares inversion of apparent resistivity pseudo-sections using quasi-Newton method Geophysical Prospecting* vol 48 p 181
- [2] Loke M H, Barker R D 1996b *Practical techniques for 3D resistivity surveys and data inversion Geophysical prospecting* vol 44 p 499
- [3] Church P, McFee J E, Gagnon S and Wort P 2006 Electrical impedance tomographic imaging of buried landmines IEEE Transaction of Geoscience and Remote Sensing vol 44 p 2407
- [4] Soleimani M, Dorn O and Lionheart W R B 2006a *A Narrow-Band Level Set Method Applied to EIT in Brain for Cryosurgery Monitoring IEEE Trans. Bio. Eng.* vol 53 No 11
- [5] Manwaring P, Halter R, Wan Y, Borsic A, Hartov A, Paulsen K 2008 *Arbitrary geometry patient interfaces for breast cancer detection and monitoring with electrical impedance tomography Conf Proc IEEE Eng Med Biol Soc.* p 1178
- [6] Gao N, Zhu S A, He B 2006 *A New Magnetic Resonance Electrical Impedance Tomography (MREIT) Algorithm: RSM-MREIT Algorithm with Applications to Estimation of Human Head Conductivity Physics in Medicine and Biology* vol 51 p 3067
- [7] McCann H, Polydorides N, Murrieta-Lee JC, Ge K, Beatty P, Pomfrett CJ 2006 *Sub-second functional imaging by electrical impedance tomography Conf Proc IEEE Eng Med Biol Soc.* p 4269
- [8] Osher S and Sethian J 1988 *Fronts propagation with curvature dependent speed: Algorithms based on hamilton-jacobi formulations J. Computational Phys.* vol 56 p 12
- [9] Sethian J A 1999 *Level Set Methods and Fast Marching Methods* (2nd ed. Cambridge, U.K.: Cambridge Univ. Press)
- [10] Santosa V 1996 *A level-set approach for inverse problems involving obstacles in ESAIM: Control, Optimization and Calculus of Variations*1 p 17
- [11] Litman A, Lesselier D and Santosa F 1998 *Reconstruction of a two-dimensional binary obstacle by controlled evolution of a level-set Inverse Prob.* vol 14 p 685
- [12] Dorn O, Miller E L and Rappaport C M 2000 *A shape reconstruction method for electromagnetic tomography using adjoint fields and level sets Inverse Prob.* vol 16 p 1119
- [13] Osher S and Paragios N 2003 *Level Set Methods in Geometric Level Set Methods in Imaging, Vision, and Graphics* (Eds. New York, NY: Springer) p 1
- [14] Polydorides N, Lionheart W R B and McCann H 2002 *Krylov subspace iterative techniques: On the detection of brain activity with EIT IEEE Trans. Med. Imag.* vol 21 no 6 p 596
- [15] Boverman G, Khames M and Miller E L 2003 *Recent work in shape-based methods for diffusive inverse problems Review of Scientific Instruments* p 2580
- [16] Chan T F and Tai X C 2004 *Level set and total variation regularization for elliptic inverse problems with discontinuous coefficients Journal of Computational Physics* p 40
- [17] Soleimani M, Lionheart W R B and Dorn O 2006b *Level set reconstruction of conductivity and permittivity from boundary electrical measurements using experimental data Inverse Problems in Science and Engineering* vol 14 No 2 p 193
- [18] Soleimani M 2007 *Level-Set Method Applied to Magnetic Induction Tomography using Experimental Data Research in Nondestructive Evaluation* vol 18 p 1
- [19] Banasiak R and Soleimani M 2010 *Shape based reconstruction of experimental data in 3D electrical capacitance tomography NDT&E International* vol 43 p 241
- [20] Adler A, Dai T and Lionheart W R B 2007 *Temporal Image Reconstruction in Electrical Impedance Tomography Physiol. Meas.*, vol 28 p 1
- [21] Cheney M, Isaacson D, Newell J C, Simske S and Goble J C 1990 *NOSER: an algorithm for solving the inverse conductivity problem Int. J. Imaging Syst. Technol.* vol 2 pp 66
- [22] Adler A, Guardo R 1996 *Electrical impedance tomography: regularized imaging and contrast detection IEEE Trans. Med. Imaging* vol 15 pp 170
- [23] Dorn O, Lesselier D 2009 *Level set methods for inverse scatteringsome recent developments Inverse Problem* vol 25 p 11
- [24] DeCezaro A, Leito A, Tai X C 2009 *On multiple level-set regularization methods for inverse problems Inverse Problem* vol 25
- [25] Irishina N, Ivarez D, Dorn O, Moscoso M 2009 *Detecting and imaging dielectric objects from real data: A shape-based approach Mathematical and Computer Modelling in press*